Optimization and implementation of piezoelectric radiators using the genetic algorithm

Mingsian R. Bai[a] and Chinghong Huang
Department of Mechanical Engineering, National Chiao-Tung University, 1001 Ta-Hsueh Road, Hsin-Chu 300, Taiwan, Republic of China

(Received 27 September 2002; revised 5 February 2003; accepted 25 February 2003)

Very thin and small (45 mm×35 mm×0.35 mm) piezoelectric radiators have been developed in this research. The system is modeled by using the energy method in conjunction with the assumed-modes method. Electrical system, mechanical system, and acoustic loading have all been accounted for during the modeling stage. On the basis of the simulation model, the genetic algorithm (GA) is employed to optimize the overall configurations for a low resonance frequency and a large gain. The resulting designs are then implemented and evaluated experimentally. Performance indices for the experimental evaluation include the frequency response, the directional response, the sensitivity, and the efficiency. It is found in the experimental results that the piezoelectric radiators are able to produce comparable acoustical output with significantly less electrical input than the voice-coil panel speakers. © *2003 Acoustical Society of America.* [DOI: 10.1121/1.1568944]

PACS numbers: 43.38.Fx, 43.38.Ja [AJZ]

I. INTRODUCTION

Miniaturization has been a major trend over the recent years in the so-called 3C industries: computer, communication, and consumer electronics. Like the other components, the loudspeakers are faced with the need to further reduce their sizes, in particular for the 3C products, e.g., personal data assistants (PDAs), mobile phones, MP3 players, etc. The panel speaker offers a potential solution to suit the above need.[1] The panel speaker provides various advantages over the conventional loudspeakers such as omnidirectivity, linearity, insensitivity to room conditions, bipolar radiation.[2] Of particular interest is that the panel speaker is planar, light, and compact, which makes it an attractive feature for many space-constrained applications. A detailed analysis and evaluation of the panel speaker can be found in Ref. 1.

Despite all the advantages, the panel speaker suffers from two drawbacks that may restrict its practical application in the 3C products. First, in the conventional design, the exciter for a panel speaker is generally the voice-coil type. The state-of-art manufacturing voice-coil exciters could reach only approximately 2 mm thickness, which is still considered too thick for many applications, such as the displays of mobile phones. Second, the electroacoustic efficiency of the conventional panel speakers driven by electromagnetic exciters was found to be quite low,[1] which raised the serious concern about the power consumption in mobile electronic products. These physical limitations associated with the conventional exciters hence motivate the development of an alternative way of excitation using a different mechanism. In this paper, planar radiators excited by piezoelectric ceramic (PZT) are proposed in an attempt to overcome the problems encountered in voice-coil exciters.[3,4] Piezoelectric ceramics can be fabricated into various shapes and thicknesses, as desired. In addition, virtually no power is consumed nor heat generated to maintain a piezoelectric actuator in an energized state. As will be manifested in the latter experimental verification, the high efficiency of piezoelectric material makes the proposed radiator an ideal device for many battery-driven products. The conversion of electrical energy into mechanical motion takes place without the generation of any magnetic field or the need for moving electrical contacts. Moreover, piezoelectric devices are capable of response times under a millisecond, limited only by the inertia of the object being moved and the output capability of the electric driver.

This paper is organized as follows. First, the energy method in conjunction with the assumed-modes method is used to derive the dynamic model of the piezoelectric radiator. The electrical system, the mechanical system, and acoustic loading have all been accounted for during the modeling stage. An electromechanical equivalent circuit is obtained for the single mode of the system. Second, on the basis of the above model, the genetic algorithm (GA) is used to optimize the design variables. Third, designs resulting from the optimization are then implemented and evaluated experimentally. Frequency response, directional response, sensitivity, and efficiency are measured in order to evaluate system performance. Finally, technical discussions and a future extension of this work are summarized.

II. DYNAMIC MODELING OF THE PIEZOELECTRIC RADIATOR

In this section, the constitutive equation of piezoelectricity is given, followed by the dynamic modeling using the energy method. Electrical system, mechanical system and acoustic loading are combined into a state-space form. The special case of the single mode of the system will also be presented in terms of an equivalent circuit.

[a]Author to whom correspondence should be addressed. Electronic mail: msbai@mail.nctu.edu.tw; telephone (03)5712121, ext. 55108.

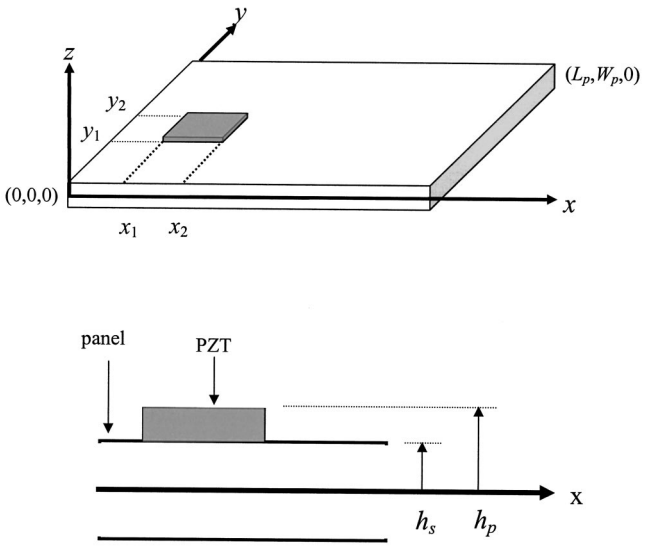

FIG. 1. Schematic diagram of the piezoelectric panel radiator. It consists of a panel and a PZT plate.

A. Energy method based on the variation principle

The model of the piezoelectric planar radiator in Fig. 1 consists of a rectangular panel and a rectangular PZT plate. Assume that the vibration of the system is small such that the nonlinear terms are negligible. The panel is of length L_P and width W_P. Let the transverse displacement of the plate be $w(x,y,t)$. The kinetic energy of the plate is

$$T_p=\frac{1}{2}\int_0^{W_p}\int_0^{L_p}\rho_p w_t^2(x,y,t)\,dx\,dy, \tag{1}$$

where ρ_p is the area density of the panel and the subscript "t" denotes the first partial derivative with respect to the time variable t. The bending strain energy of the plate is[5]

$$U_p=\frac{1}{2}D\int_0^{W_p}\int_0^{L_p}[w_{xx}^2+w_{yy}^2+2\upsilon w_{xx}w_{yy} +2(1-\upsilon)w_{xy}^2]dx\,dy, \tag{2}$$

where $D=Eh^3/12(1-\upsilon^2)$ is the bending stiffness of the panel, $h=2h_s$ is the thickness of the panel, E is the Young's modulus of the panel, and υ is the Poisson's ratio of the panel. The subscript "xx" denotes the second partial derivative with respect to the space coordinate x; a similar rule applies to the other variables. It should be clear from the context, where all subscripts in the following equations that are not in the definition of the variable should be interpreted as differentiation with respect to the variable.

On the other hand, the internal energy of the PZT plate needs to be established. The formulation is based on the h-form constitutive equations. For our problem at hand, the constitutive equations of a hexagonal crystal class (6 mm) PZT plate can be written as

$$\begin{bmatrix}T_1\\T_2\\T_6\\E_3\end{bmatrix}=\begin{bmatrix}c_{11}^D & c_{12}^D & 0 & -h_{31}\\ c_{12}^D & c_{11}^D & 0 & -h_{31}\\ 0 & 0 & c_{66}^D & 0\\ -h_{31} & -h_{31} & 0 & \beta_{33}^S\end{bmatrix}\begin{bmatrix}S_1\\S_2\\S_6\\D_3\end{bmatrix}, \tag{3}$$

where T is the stress, S is the strain D is the dielectric displacement, E is the field strength, h is the piezoelectric voltage constant, c^D is the elastic stiffness under the condition of constant dielectric displacement, and β^S is the impermittivity under the condition of constant strain, the subscripts signify the orientation of electrical and mechanical quantities, and $c_{66}^D=(c_{11}^D-c_{12}^D)/2$. From the thin-plate theory, $S_1=-zw_{xx}$, $S_2=-zw_{yy}$, and $S_6=-2zw_{xy}$. The internal energy of the piezoelectric material U_c can be expressed as[6]

$$\begin{aligned}U_c&=\frac{1}{2}\int_V[(T_1S_1+T_2S_2+T_6S_6)+E_3D_3]dV,\\ &=\frac{1}{2}\left\{\int_{y_1}^{y_2}\int_{x_1}^{x_2}[c_{11}^D I_1(w_{xx}^2+w_{yy}^2)+2c_{12}^D I_1 w_{xx}w_{yy}\right.\\ &\quad+2h_{31}D_3I_2(w_{xx}+w_{yy})+4c_{66}^D I_1 w_{xy}^2]dx\,dy\\ &\quad\left.+\beta_{33}^S V_c D_3^2\right\},\end{aligned} \tag{4}$$

where $I_1=(h_p^3-h_s^3)/3$, $I_2=(h_p^2-h_s^2)/2$, and $V_c=W_cL_c(h_p-h_s)$ is the volume of PZT. W_c and L_c are the width and the length of PZT. The virtual work done by the noninertial forces and the external voltage is written as

$$\begin{aligned}\delta W&=\int_{y_1}^{y_2}\int_{x_1}^{x_2}V_a(t)\,\delta D_3\,dx\,dy\\ &\quad+\int_0^{W_p}\int_0^{L_p}f(x,y,t)\,\delta w\,dx\,dy\\ &=V_a\,\delta D_3\,A_c+\int_0^{W_p}\int_0^{L_p}f(x,y,t)\,\delta w\,dx\,dy,\end{aligned} \tag{5}$$

where $A_c=W_cL_c$, and V_a is the applied voltage to the PZT.

B. Assumed-modes method

The assumed-modes method is then employed in deriving the discretized equation of motion.[7] In this method, the continuous system is approximated as an n-degree-of-freedom system, where the displacement satisfies

$$w(x,y,t)=\sum_{i=1}^{n}\phi_i(x,y)q_i(t), \tag{6}$$

where $\phi_i(x,y)$ are *admissible functions* and $q_i(t)$ are the *principal coordinates*.[7] Using the series expansion, the energy terms shall be discretized in terms of the principal coordinates. The kinetic energy can be expressed as

$$T_p=\frac{1}{2}\sum_{i=1}^{n}\sum_{j=1}^{n}m_{ij}\dot{q}_i(t)\dot{q}_j(t), \tag{7}$$

where

$$m_{ij}=\rho_p\int_0^{W_p}\int_0^{L_p}\phi_i(x,y)\,\phi_j(x,y)\,dx\,dy \tag{8}$$

are symmetric mass coefficients. In a similar fashion, the strain energy of the panel can be written as

$$U_p=\frac{1}{2}\sum_{i=0}^{n}\sum_{j=0}^{n}k_{ij}^{p}q_i(t)q_j(t), \tag{9}$$

where

$$\begin{aligned}k_{ij}^{p}=D\int_0^{W_p}\int_0^{L_p}&[\phi_{i,xx}(x,y)\,\phi_{j,xx}(x,y)\\&+\phi_{i,yy}(x,y)\,\phi_{j,yy}(x,y)+2\upsilon\phi_{i,xx}(x,y)\,\phi_{j,yy}(x,y)\\&+2(1-\upsilon)\phi_{i,xy}(x,y)\,\phi_{j,xy}(x,y)]k\,dx\,dy.\end{aligned} \tag{10}$$

The internal energy of the PZT can also be expressed as

$$\begin{aligned}U_c=&\frac{1}{2}\sum_{i=0}^{n}\sum_{j=0}^{n}k_{ij}^{c}q_i(t)q_j(t)+\frac{1}{2}\sum_{i=0}^{n}\alpha_i q_i(t)D_3\\&+\tfrac{1}{2}V_c\beta_{33}^{S}D_3^2,\end{aligned} \tag{11}$$

where

$$\begin{aligned}k_{ij}^{c}=\int_{y_1}^{y_2}\int_{x_1}^{x_2}&I_1\{c_{11}^{D}[\phi_{i,xx}(x,y)\,\phi_{j,xx}(x,y)\\&+\phi_{i,yy}(x,y)\,\phi_{ji,yy}(x,y)]\\&+2c_{12}^{D}\phi_{i,xx}(x,y)\,\phi_{j,yy}(x,y)\\&+4c_{66}^{D}\phi_{i,xy}(x,y)\,\phi_{j,xy}(x,y)\}dx\,dy,\end{aligned} \tag{12}$$

$$\alpha_i=2h_{31}I_2\int_{y_1}^{y_2}\int_{x_1}^{x_2}[\phi_{i,xx}(x,y)+\phi_{i,yy}(x,y)]dx\,dy. \tag{13}$$

The virtual energy is written as

$$\delta W=A_c V_a\,\delta D_3+\sum_{i=0}^{n}f_i\,\delta q_i(t), \tag{14}$$

where

$$f_i=\int_0^{W_p}\int_0^{L_p}f(x,y,t)\,\phi_i(x,y)\,dx\,dy \tag{15}$$

are modal forces. Let

$$k_{ij}^{t}=k_{ij}^{p}+k_{ij}^{c}, \tag{16}$$

and k_{ij} are symmetric stiffness coefficients. The dielectric displacement $D_3=D_3(t)$ in the z axis is assumed to be constant on the electrodes and is a function of time because in our application the problem can be treated as electrostatic.

C. The Lagrange equation

The introduction of the assumed modes to the energy terms in the early stage rather than to the differential equations offers great convenience. The discretized energy terms are then substituted into the Lagrange equation,

$$\frac{d}{dt}\left(\frac{\partial L}{\partial\dot{q}_i}\right)-\frac{\partial L}{\partial q_i}=f_i,\quad i=1,2,...,n, \tag{17}$$

$$-\frac{\partial L}{\partial D_3}=A_c V_a, \tag{18}$$

where $L=T_p-U_p-U_c$ is the *Lagrangian*. The substitution leads directly to the following dynamic equations:

$$\sum_{j=1}^{n}m_{ij}\ddot{q}_j(t)+\sum_{j=1}^{n}k_{ij}^{t}q_j(t)+\frac{\alpha_i}{A_c}Q=f_i,\quad i=1,2,...,n, \tag{19}$$

$$\frac{1}{A_c}\sum_{j=1}^{n}\alpha_j q_j(t)+\frac{t_c}{A_c}\beta_{33}^{S}Q=V_a, \tag{20}$$

where t_c is the thickness of PZT and $D_3=Q/A_c$, with Q being the electric charges on the electrodes. These equation can be written in a matrix form:

$$\mathbf{M}\ddot{\mathbf{q}}+\mathbf{K}\mathbf{q}+\boldsymbol{\alpha}Q=\mathbf{f}, \tag{21}$$

$$\boldsymbol{\gamma}^T\mathbf{q}+\lambda Q=V_a, \tag{22}$$

where $\mathbf{M}=[m_{ij}]$, $\mathbf{K}=[k_{ij}^{t}]$, $\boldsymbol{\alpha}=[\alpha_i/A_c]$, $\boldsymbol{\gamma}=[\alpha_j/A]$, and $\lambda=t\beta_{33}^{S}/A_c$.

To account for the effects of electrical circuit,

$$V_a=V_s-R\dot{Q}-L\ddot{Q}, \tag{23}$$

where V_s is the source voltage, R and L are the equivalent resistance and the inductance, respectively. Equations (21) and (22) can be assembled into a state-space form:

$$\begin{aligned}\frac{d}{dt}\begin{bmatrix}\mathbf{q}\\Q\\\dot{\mathbf{q}}\\Q\end{bmatrix}=&\begin{bmatrix}0&0&1&0\\0&0&0&1\\-\mathbf{M}^{-1}\mathbf{K}&-\mathbf{M}^{-1}\boldsymbol{\alpha}&0&0\\-\frac{1}{L}\boldsymbol{\gamma}^T&-\frac{\lambda}{L}&0&-\frac{R}{L}\end{bmatrix}\begin{bmatrix}\mathbf{q}\\Q\\\dot{\mathbf{q}}\\Q\end{bmatrix}\\&+\begin{bmatrix}0&0\\0&0\\\mathbf{M}^{-1}&0\\0&\frac{1}{L}\end{bmatrix}\begin{bmatrix}\mathbf{f}\\V_s\end{bmatrix}.\end{aligned} \tag{24}$$

D. Acoustic loading

In addition to the electrical system and the mechanical system, the acoustic loading is also considered in the modeling. In physical coordinates, the relationship between the sound pressure and the surface velocity can be approximated in a discrete form,

$$\mathbf{p}=\mathbf{Z_A}\mathbf{v}, \tag{25}$$

where $\mathbf{p}$ is the sound pressure vector, $\mathbf{v}$ is the surface velocity vector, and $\mathbf{Z_A}$ is the *radiation impedance matrix*:[8]

$$\mathbf{Z_A} = \rho_p c_s \begin{bmatrix} 1-e^{-jk\sqrt{A/\pi}} & \frac{jkA}{2\pi}\frac{e^{-jkr_{12}}}{r_{12}} & \cdots & \frac{jkA}{2\pi}\frac{e^{-jkr_{1n}}}{r_{1n}} \\ \frac{jkA}{2\pi}\frac{e^{-jkr_{21}}}{r_{21}} & 1-e^{-jk\sqrt{A/\pi}} & \cdots & \vdots \\ \vdots & \vdots & \ddots & \vdots \\ \frac{jkA}{2\pi}\frac{e^{-jkr_{m1}}}{r_{m1}} & \cdots & \cdots & 1-e^{-jk\sqrt{A/\pi}} \end{bmatrix}, \tag{26}$$

in which $r_{mn}=r_{nm}$ is the distance from the element m to the element n, $1\leqslant m$, $n\leqslant N$, and $k=\omega/c_s$ is the wave number, with c_s being the speed of sound. A is the area of each element.

Rewrite the assumed-modes expansion of Eq. (6) in the matrix form

$$\mathbf{w}=\mathbf{\Phi q}, \tag{27}$$

where $\mathbf{\Phi}=\lfloor\phi_{ij}(x,y)\rfloor$, in which $\phi_{ij}(x,y)$ is the admissible function of the ijth mode. $\mathbf{w}$ and $\mathbf{q}$ are defined as the physical and modal displacement vectors, respectively, on the panel surface. $\mathbf{\Phi}$ is the transformation matrix that relates the physical space and the modal space. Using the matrix $\mathbf{\Phi}$, Eq. (25) can be transformed into the modal space. Let $\tilde{\mathbf{p}}$ and $\tilde{\mathbf{v}}$ be the surface pressure and velocity in the modal space,

$$\mathbf{p}=\mathbf{\Phi}\tilde{\mathbf{p}}, \tag{28}$$

$$\mathbf{v}=\mathbf{\Phi}\tilde{\mathbf{v}}. \tag{29}$$

Hence, we have

$$\tilde{\mathbf{p}}=\tilde{\mathbf{Z}}_\mathbf{A}\tilde{\mathbf{v}}, \tag{30}$$

where the modal radiation impedance,

$$\tilde{\mathbf{Z}}_\mathbf{A}=\mathbf{\Phi}^{-1}\mathbf{Z_A}\mathbf{\Phi}. \tag{31}$$

To obtain the frequency response function, we let

$$\tilde{\mathbf{v}}=j\omega\mathbf{q}. \tag{32}$$

Substituting Eqs. (30) and (32) into Eqs. (21) and (22) yields the dynamic equations in the modal space:

$$\left[\lambda\left(j\omega\mathbf{M}+\mathbf{MU}+\frac{1}{j\omega}\mathbf{K}+A\tilde{\mathbf{Z}}_A\right)-\frac{1}{j\omega}\boldsymbol{\alpha}\boldsymbol{\gamma}^T\right]\tilde{\mathbf{v}}=-\boldsymbol{\alpha}V_\mathbf{a}, \tag{33}$$

where $\omega_{n,ij}$ is the natural frequency in the ijth mode and an *ad hoc* damping matrix. $\mathbf{U}=\mathrm{diag}\lfloor 2\zeta\omega_{n,ij}\rfloor$ is introduced, with ζ being the damping ratio.

E. Equivalent circuit

To facilitate the ensuing optimal design, a special case, the single-mode system, is considered. For a single mode, generally the fundamental mode, Eqs. (6), (21), and (22), are rewritten as

$$w(x,y,t)=\phi(x,y)q(t), \tag{34}$$

$$m\ddot{q}+kq+\alpha Q=f, \tag{35}$$

$$\alpha q+\lambda Q=V_a, \tag{36}$$

where $m=\rho_p$ if $\|\phi\|_2=1$.

$$k^t=D\int_0^{W_p}\int_0^{L_p}[\phi_{xx}^2+\phi_{yy}^2+2\upsilon\phi_{xx}\phi_{yy}+2(1-\upsilon)\phi_{xy}^2]dx\,dy + \int_{y_1}^{y_2}\int_{x_1}^{x_2}[c_{11}^D I_1\phi_{xx}^2+2c_{12}^D I_1\phi_{xx}\phi_{yy}+c_{11}^D I_1\phi_{yy}^2 + 4c_{66}^D I_1\phi_{xy}^2]dx\,dy, \tag{37}$$

$$\alpha=\frac{\alpha_1}{A_c}=\frac{2h_{31}I_2}{A_c}\int_{y_1}^{y_2}\int_{x_1}^{x_2}(\phi_{xx}+\phi_{yy})dx\,dy, \tag{38}$$

$$\lambda=\frac{h_s-h_p}{A_c}\beta_{33}^S. \tag{39}$$

Assuming a time-harmonic analysis, the velocity and the electric current can be related, respectively, to the displacement and the electric charge,

$$q=\frac{u}{j\omega}, \tag{40}$$

$$Q=\frac{I}{j\omega}. \tag{41}$$

Let $k=1/C_M$, $\tau=\alpha C_E$, and $\lambda=1/C_E$. Equations (35) and (36) become

$$j\omega mu+\frac{1}{j\omega C_M}u+\frac{\tau}{j\omega C_E}I=f, \tag{42}$$

$$\frac{\tau}{j\omega C_E}u+\frac{1}{j\omega C_E}I=V_a, \tag{43}$$

where C_M and C_E denote the mechanical compliance and the electrical capacitance of PZT. Or, in a matrix form,

$$\begin{bmatrix} j\omega m+\frac{1}{j\omega C_M} & \frac{\tau}{j\omega C_E} \\ \frac{\tau}{j\omega C_E} & \frac{1}{j\omega C_E} \end{bmatrix}\begin{bmatrix} u \\ I \end{bmatrix}=\begin{bmatrix} f \\ V_a \end{bmatrix}. \tag{44}$$

As evidenced from the symmetric impedance matrix, the piezoelectric radiator is a ''reciprocal'' transducer. With *ad hoc* damping introduced, the electromechanical equivalent circuit is shown in Fig. 2(a). Reflecting the electrical side to the mechanical side gives Fig. 2(b), where

$$C_M'=\frac{C_M}{1-K^2}, \tag{45}$$

and $K=\sqrt{\alpha^2 C_M C_E}$ being the coupling factor. From the equivalent circuit, the frequency response between the modal velocity and the applied voltage can be expressed as

$$\frac{u}{V_a}=\frac{(j\omega)^2 C_E\tau}{(j\omega)^2 m+(j\omega)(R+Z_A)+\frac{1}{C_T}}, \tag{46}$$

where $C_T=C_E C_M'/(C_E+\tau^2 C_M')$ and $R=2m\zeta\sqrt{1/mC_T}$, with ζ being the damping ratio. This single-mode approximation is apparently a second-order system with the natural frequency,

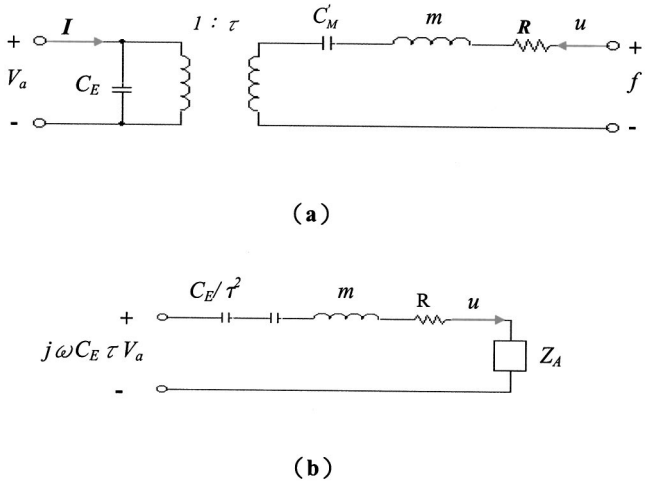

FIG. 2. Electromechanical equivalent circuits of the piezoelectric panel radiator. (a) The electromechanical equivalent circuit; (b) the equivalent circuit referred to as the mechanical side.

$$\omega_0 = \sqrt{\frac{1}{mC_T}}, \tag{47}$$

and a gain beyond resonance

$$g_\infty = \left|\frac{u}{V_a}\right| \approx \frac{C_E \tau}{m}, \quad \omega \gg \omega_0 . \tag{48}$$

An example of the single-mode frequency response of the piezoelectric radiator is illustrated in Fig. 3. For good performance, it is desirable for the resulting design of the radiator to have a low natural frequency ω_0 and high gain g_∞.

III. OPTIMAL DESIGN VIA THE GENETIC ALGORITHM

The genetic algorithm (GA) is an optimization algorithm that is originally motivated by natural selection and evolutionary genetics.[9] The GA has proven to be efficient in many areas such as function optimization and image processing. Unlike the conventional gradient search algorithms, the GA requires no calculation of the gradient and is not susceptible to problems of local minima. In each ''generation,'' three basic genetic operators, *reproduction*, *crossover*, and *mutation*, are performed to generate a new population and *fitness* functions of the *chromosomes* of the population are evaluated. An optimal solution is then obtained, according to the principle of ''survival of the fittest.'' The GA procedure applied to design the piezoelectric radiator is detailed as follows.

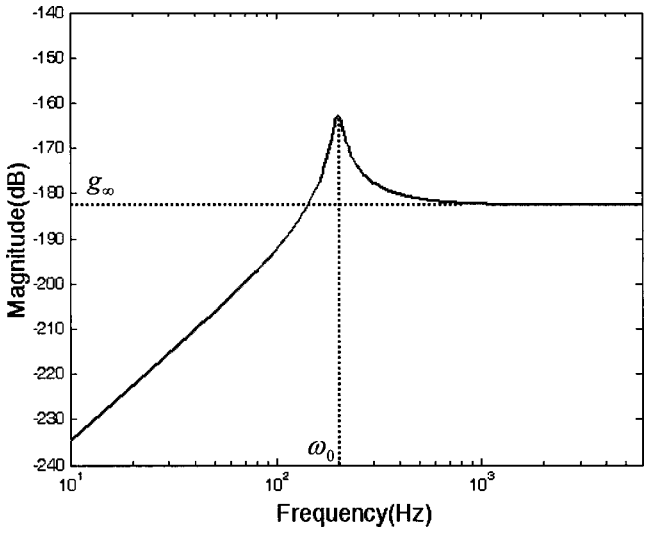

FIG. 3. The example of the single-mode frequency response of the piezoelectric panel radiator. ω_0 is the natural frequency and g_∞ is the gain beyond resonance.

A. Fitness function

Fitness is a measure of the survival rate of a chromosome. A chromosome with high fitness has a high probability of reproducing one or more offspring in the next generation. The ratio of the gain and the natural frequency of the single-mode approximation serves as the fitness function for the GA optimization:

$$f_c = \frac{g_\infty}{\omega_0} = \frac{\frac{C_E \tau}{m}}{\frac{1}{\sqrt{mC_T}}} = \alpha C_E^2 \sqrt{\frac{C_T}{m}}. \tag{49}$$

The goal of optimization is to search for a design with a low natural frequency and a high gain by maximizing the fitness function f_c. In the single-mode system, parameters relevant to the optimization are

$$m = \rho_p , \tag{50}$$

$$C_E = \frac{1}{\lambda} = \frac{L_c W_c}{t_c \beta_{33}^S}, \tag{51}$$

$$C_T = \frac{C_E C_M'}{C_E + \tau^2 C_M'} = C_M = \frac{1}{k}, \tag{52}$$

$$\alpha = -6 \frac{h_{31}(t_p t_c + t_c^2)}{\sqrt{L_c W_c}} \left[\left(\frac{1}{L_c^2} + \frac{1}{W_c^2} \right) \cos \frac{\pi x_1}{L_c} \cos \frac{\pi y_1}{W_c} \right], \tag{53}$$

$$k^t = \pi^4 \left[D + \left(\frac{1}{2} t_p^2 t_c + t_p t_c^2 + \frac{2}{3} t_c^3 \right) c_{11}^D \right] \left(\frac{1}{L_c^4} + \frac{1}{W_c^4} + \frac{2}{L_c^2 W_c^2} \right). \tag{54}$$

The symbols t_p and t_c are the thickness of the panel and PZT, respectively. Substituting Eqs. (50)–(53) into Eq. (49) gives

$$f_c = \alpha C_E^2 \sqrt{\frac{C_T}{m}} = \eta \frac{t_p + t_c}{t_t} L_c W_c \frac{1}{\sqrt{k}}, \tag{55}$$

where

$$\eta = -6 \frac{h_{31}}{\beta_{33}^S} \sqrt{\frac{L_c W_c}{m}} \left(\frac{1}{L_c^2} + \frac{1}{W_c^2} \right) \cos \frac{\pi x_1}{L_c} \cos \frac{\pi y_1}{W_c}. \tag{56}$$

When $0 \leqslant x_1 \leqslant W_p/2$ and $0 \leqslant x_2 \leqslant L_p/2$, η is a positive constant. It can be readily verified that

$$\partial f_c / \partial L_c > 0, \tag{57}$$

$$\partial f_c / \partial W_c > 0, \tag{58}$$

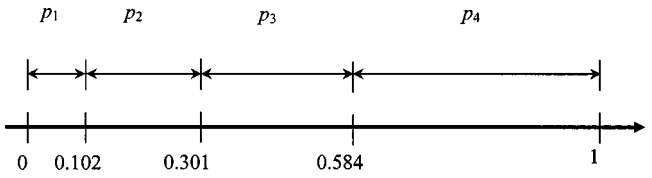

FIG. 4. The reproduction probabilities of four chromosomes, c_1-c_4, with fitness functions, 17, 33, 47, and 69, are concatenated in a real line.

$$\partial f_c/\partial t_c<0. \tag{59}$$

Thus, f_c is a monotonically increasing function of L_c and W_c, and a monotonically decreasing function of t_c. That is, it is generally preferable to have a design using a large and thin PZT, provided no other constraints are of concern. In what follows, the parameter L_c, W_c, and t_c will not be optimized, but were constrained in a certain prescribed range.

B. Encoding and decoding

Suppose that the position of the PZT, (x_1,y_1), on the panel are to be optimized. The variables x_1 and y_1 are encoded into a binary string of length l_i, called a chromosome. The resolution for the string of such length is

$$R_i=\frac{x_i^U-x_i^L}{2^{l_i}-1}, \tag{60}$$

where x_i^U and x_i^L are the upper and lower limits of the parameter. For example, if $0<x_1<4.5$ mm, $0<y_1<3.5$ mm, and the desired resolutions are $R_1=0.145$ and $R_2=0.113$, then $l_1=l_2=5$. If $x_1=1.595$ and $y_1=1.468$, then the chromosome is encoded as [01011 01101].

C. Reproduction, crossover, and mutation

Reproduction directs the search of GA toward the best individuals. The chromosome of the current population is reproduced in the next generation according to the reproduction probability p_i,

$$p_i=\frac{f_c}{\Sigma_1^{P_l} f_c}, \tag{61}$$

where P_l is the population size. Assume there are four chromosomes, c_1-c_4, in the zero generation with fitness functions 17, 33, 47, and 69. From Eq. (61), the reproduction probabilities are $p_1=0.102$, $p_2=0.199$, $p_3=0.283$, and $p_4=0.416$, respectively. The chromosome c_4 is the most likely to reproduce in the next generation. These four reproduction probabilities are then concatenated in the real line, as shown in Fig. 4. In the first generation, four random numbers between 0 and 1 are generated. For example, if the generated random numbers are 0.812, 0.666, 0.111, and 0.501, the candidate chromosomes for reproduction in the next generation will be c_4, c_4, c_2, and c_3, respectively.

Crossover is intended to exchange the information between chromosomes via a probabilistic decision in the mating pool. It proceeds in three steps. First, the crossover rate p_c is specified (usually $0.8<p_c<1$, and we choose $p_c=0.9$). Two chromosomes in the mating pool are selected to cross over at random. Precisely, the entire population in each generation is divided into pairs, e.g., 100 pairs would be required for 200 chromosomes. For each pair, a random number between 0 and 1 is then generated. If the random number is less than the crossover rate p_c, the crossover procedure will take place. Second, a splice point at the chromosome is selected randomly. Third, the genetic codes after the splice point are interchanged. For example, there are two chromosomes c_1 and c_2 with the splice point at the third bit: $c_1=010_\Delta 1010$, $c_2=111_\Delta 1111$. With crossover, two new chromosomes are generated: $\tilde{c}_1=010_\Delta 1111$, $\tilde{c}_2=111_\Delta 1010$.

Reproduction and crossover provide the most search power for GA. However, the gene becomes increasingly homogeneous as one gene begins to dominate after several generations and eventually results in premature convergence. To obviate this problem, mutation is introduced into the GA procedure. Let the probability of mutation be p_m (usually $0<p_m<0.01$, and we choose $p_m=0.01$). This probability determines how many genes are selected for mutation in each generation. In this analysis, where the population was chosen to be 200 at the given 0.01 mutation rate, approximately two genes were presumably selected for mutation in each generation. Mutation is carried out by alternating the gene from zero to one, or from one to zero, with the mutation point determined randomly. For instance, a chromosome c_3 with the mutation point at the third bit is $\tilde{c}_3=10\underset{\Delta}{0}\,101010$. After mutation, the chromosome becomes $\tilde{c}_3=10\underset{\Delta}{1}\,101010$. Note, however, that mutation should be used sparingly. The GA would behave like a random search if the mutation rate is too high.

The aforementioned GA procedure was applied to the design of the piezoelectric radiator. The parameters to optimize include the positions of the PZT and the Young's modulus of the panel. Two kinds of thickness (100 and 150 μm) and five kinds of aspect ratio were examined in the optimization. The results of optimal PZT positions on the panel are

TABLE I. The results of optimal PZT positions on the panel obtained using the GA procedure. Every entry in the table includes three values: the gain beyond resonance, the natural frequency, and the optimal position of the PZT.

		The thickness of PZT	
		100 μm	150 μm
Aspect ratio (length=1.5 cm)	1:(1/3)	−179.520 dB 147.461 Hz (1 cm, 2.75 cm)	−181.886 dB 179.076 Hz (1 cm, 2.81 cm)
	1:(1/2)	−172.512 dB 163.710 Hz (1 cm, 2.65 cm)	−174.870 dB 205.458 Hz (1 cm, 2.61 cm)
	1:1	−160.639 dB 202.512 Hz (1 cm, 2.27 cm)	−163.003 dB 265.580 Hz (1 cm, 2.32 cm)
	1:2	−149.287 dB 248.890 Hz (1 cm, 1.46 cm)	−151.643 dB 335.386 Hz (1 cm, 1.5 cm)
	1:3	−143.437 dB 265.826 Hz (1 cm, 0.75 cm)	−145.812 dB 359.739 Hz (1 cm, 0.78 cm)

summarized in Table I. Every entry in the table includes three values: the gain beyond resonance, the natural frequency, and the optimal position of the PZT. The optimal Young's moduli of the panel are found to vary between 9 and 13 GPa.

IV. NUMERICAL SIMULATION

Although the assumed-modes method, in principle, is applicable to general cases, the modes we assumed are restricted to the eigenfunctions of a simply supported plate that are simple enough for a practical calculation during optimization. The simply supported boundary conditions are

$$w(0,y)=w(L_p,y)=\frac{\partial^2 w}{\partial x^2}(0,y)=\frac{\partial^2 w}{\partial x^2}(L_p,y)=0, \quad 0\leqslant y\leqslant W_p, \tag{62}$$

$$w(x,0)=w(x,W_p)=\frac{\partial^2 w}{\partial y^2}(x,0)=\frac{\partial^2 w}{\partial y^2}(x,W_p)=0, \quad 0\leqslant x\leqslant L_p. \tag{63}$$

The associated eigenfunctions are

$$\phi_{mn}(x,y)=\frac{2}{\sqrt{L_pW_p}}\sin\frac{m\pi x}{L_p}\sin\frac{n\pi y}{W_p}. \tag{64}$$

The natural frequencies are

$$\omega_{mn}=\sqrt{\frac{D}{\rho_p}}\pi^2\left(\frac{m^2}{L_c^2}+\frac{n^2}{W_c^2}\right). \tag{65}$$

Suppose that only M most significant modes are retained in the series expansion. A $M\times M$ transformation matrix $\mathbf{\Phi}$ can be constructed by dividing the panel into M grid points:

$$\mathbf{\Phi}=\frac{2}{\sqrt{L_pW_p}}\begin{bmatrix} \frac{1}{N_1}\sin\frac{m_1\pi x_1}{L_p}\sin\frac{n_1\pi y_1}{W_p} & \cdots & \frac{1}{N_M}\sin\frac{m_M\pi x_1}{L_p}\sin\frac{n_M\pi y_1}{W_p} \\ \vdots & \ddots & \vdots \\ \frac{1}{N_1}\sin\frac{m_1\pi x_M}{L_p}\sin\frac{n_1\pi y_M}{W_p} & \cdots & \frac{1}{N_M}\sin\frac{m_M\pi x_M}{L_p}\sin\frac{n_M\pi y_M}{W_p} \end{bmatrix}, \tag{66}$$

where N_i is the norm of the ith column. Hence, the modal radiation impedance $\tilde{\mathbf{Z}}_\mathbf{A}$ is obtained using Eq. (31). The modal velocity vector $\tilde{\mathbf{v}}$ is obtained by solving Eq. (33). The velocity in physical space is then obtained from Eq. (29).

For radiators in a planar baffle, the propagation matrix $\mathbf{E}$ can be written as[8]

$$\mathbf{E}=j\frac{\rho_0 c_s kA}{2\pi}\begin{bmatrix} \frac{e^{-jkr_{11}}}{r_{11}} & \frac{e^{-jkr_{12}}}{r_{12}} & \cdots & \frac{e^{-jkr_{1n}}}{r_{1n}} \\ \frac{e^{-jkr_{21}}}{r_{21}} & \frac{e^{-jkr_{22}}}{r_{22}} & \cdots & \frac{e^{-jkr_{2n}}}{r_{2n}} \\ \vdots & \vdots & \ddots & \vdots \\ \frac{e^{-jkr_{m1}}}{r_{m1}} & \frac{e^{-jkr_{m2}}}{r_{m2}} & \cdots & \frac{e^{-jkr_{mn}}}{r_{mn}} \end{bmatrix}, \tag{67}$$

where A is the area of each element and r_{mn} is the distance from the element n to the field point m. Using the matrix $\mathbf{E}$, we can calculate the farfield pressure,

$$\mathbf{p_f}=\mathbf{Ev}, \tag{68}$$

where $\mathbf{v}$ is the surface velocity vector on the panel.

The data of the PZT and the panel in our simulation are shown in Table II. The dimensions of the panel are 45 mm $\times$35 mm$\times$0.1 mm, which are close to those of a cellular phone. Assume that the panel material is polycarbonate (PC). The size of the PZT is 15 mm$\times$30 mm$\times$0.1 mm. Using the GA procedure with a population size 200, the optimal position of the PZT on the PC panel was found to be at (10.0 mm, 14.6 mm). The learning curve of the GA is shown in Fig. 5. With approximately 100 iterations, the fitness function settles to 2.6×10^{-10}. The computation time was nearly 4 hours for 300 iterations on a Pentium 4 personal computer. The frequency responses for the optimal position and a nonoptimal position (15.0 mm, 10.0 mm) of the PZT, of the on-axis sound pressure at a point 0.5 m away from the panel, were calculated using the forgoing numerical model and compared in Fig. 6. The configuration with the optimal PZT position exhibits significantly better low-frequency response and high-frequency gain as well.

V. EXPERIMENTAL INVESTIGATION

Experiments were undertaken to verify the proposed optimal designs of the piezoelectric panel radiators. Two kinds of panel materials, the polycarbonate and the carbon fiber composite material, are used in the experiment. The parameters of panel materials are listed in Table III. A PU foam and

TABLE II. The data of the PZT and the panel used in the simulation. The dimensions of the panel are 45 mm$\times$35 mm$\times$0.1 mm.

	Parameter	Value
PC plate	Size	0.045 m$\times$0.035 m$\times$0.00025 m
	Density	1200 kg/m^3
	Young's modulus	2.7 GPa
	Poisson's ratio	0.97
PZT	Size	0.0015 m$\times$0.0030 m$\times$0.0001 m
	β_{33}^S	1.94×10^8
	h	-8.1×10^8 V/m
	c_{11}^D	11.73×10^{10} N/m^2
	c_{12}^D	7.77×10^{10} N/m^2
	c_{66}^D	1.98×10^{10} N/m^2

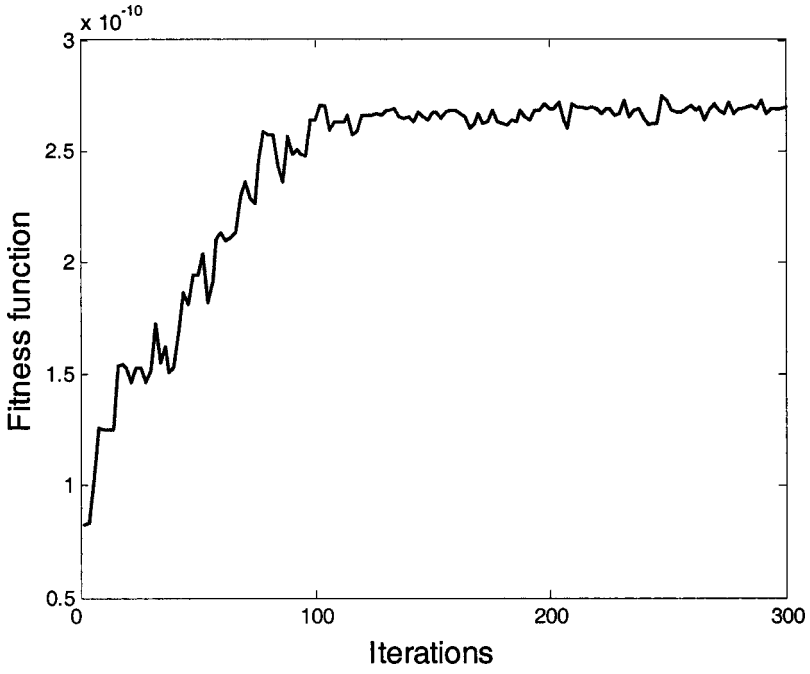

FIG. 5. The learning curve of the GA. With approximately 100 iterations, the fitness function settles to 2.6 $\times 10^{-10}$. The computation time was nearly 4 h for 300 iterations on a Pentium 4 personal computer.

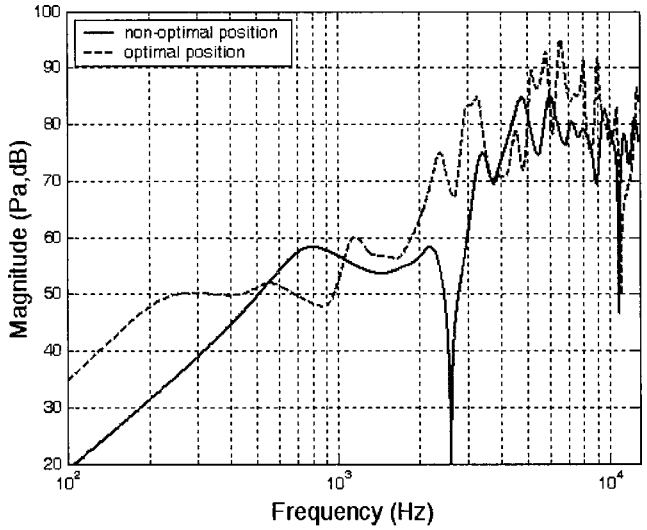

FIG. 6. The simulated on-axis frequency responses for two positions of the PZT, at a point 0.5 m away from the panel. The size of the panel is 45 mm$\times$35 mm$\times$0.25 mm. The size of the PZT is 15 mm$\times$30 mm $\times$0.1 mm. The optimal position of the PZT is at (10.0 mm, 14.6 mm). The nonoptimal position of the PZT is at (15.0 mm, 10.0 mm).

TABLE III. The parameters of the polycarbonate material and the carbon fiber composite material.

	Polycarbonate (PC)	Carbon fiber composite material
Density (ρ, kg/m^3)	1200	1546.37
Young's modulus (E, GPa)	2.7	$E_1=147.564$, $E_2=9.314$
Poisson's ratio (ν)	0.97	0.283
Shear modulus (G, GPa)	0.42	5.702

TABLE IV. Configurations of piezoelectric radiators investigated in the experiment. Two kinds of suspensions, a PU foam and a plastic tape, are tested.

No. of panel	T size (mm)	Panel size (mm)	Material of plate	Material of BC	PZT position
No. 1	15$\times$30$\times$0.1	45$\times$35$\times$0.25	PC	PU foam ($t=1$ mm)	Nonoptimal: (15.0 mm, 10.0 mm)
No. 2	15$\times$30$\times$0.1	45$\times$35$\times$0.25	PC	PU foam ($t=1$ mm)	Optimal: (10.0 mm, 14.6 mm)
No. 3	15$\times$30$\times$0.1	45$\times$35$\times$0.25	Carbon fiber (0°$\times$2)	PU foam ($t=1$ mm)	Optimal: (10.0 mm, 14.6 mm)
No. 4	15$\times$30$\times$0.1	45$\times$35$\times$0.25	Carbon fiber (0°$\times$2)	Adhesive tape	Optimal: (10.0 mm, 14.6 mm)

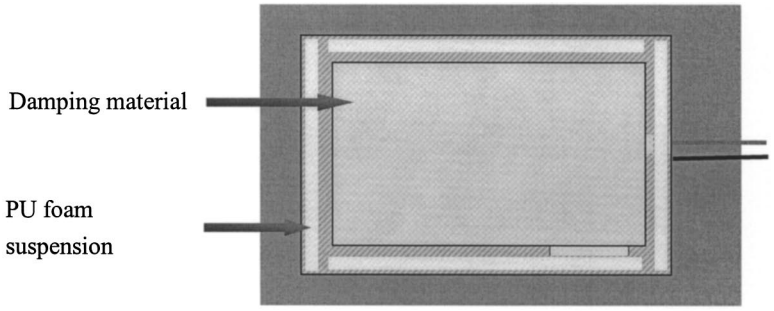

(a)

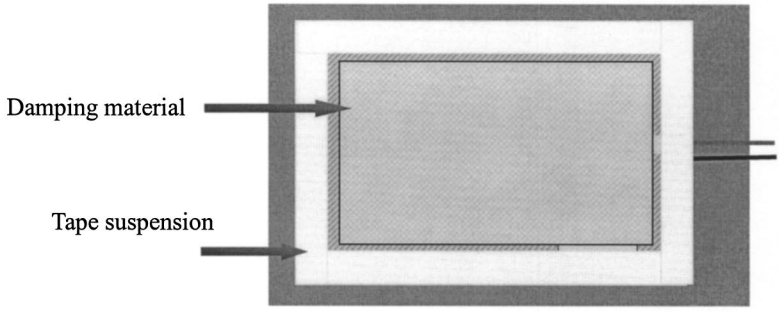

(b)

FIG. 7. Illustrations of the piezoelectric radiators. (a) Nos. 1, 2 and 3; (b) No. 4.

a plastic tape, representing a hard suspension and a soft suspension, are tested. The suspensions are sealed all around the boundary of the panels. With an appropriate combination of these conditions, four configurations of piezoelectric radiators were investigated in the experiment, as summarized in Table IV. The implemented piezoelectric panel radiators are schematically shown in Fig. 7. The panels were treated with some damping. Figure 8 shows the photo of the radiator No. 2. All radiators were embedded in a baffle while testing. The experimental arrangement is shown in Fig. 9. The performance of the panel radiators are measured in an anechoic room and summarized as follows.

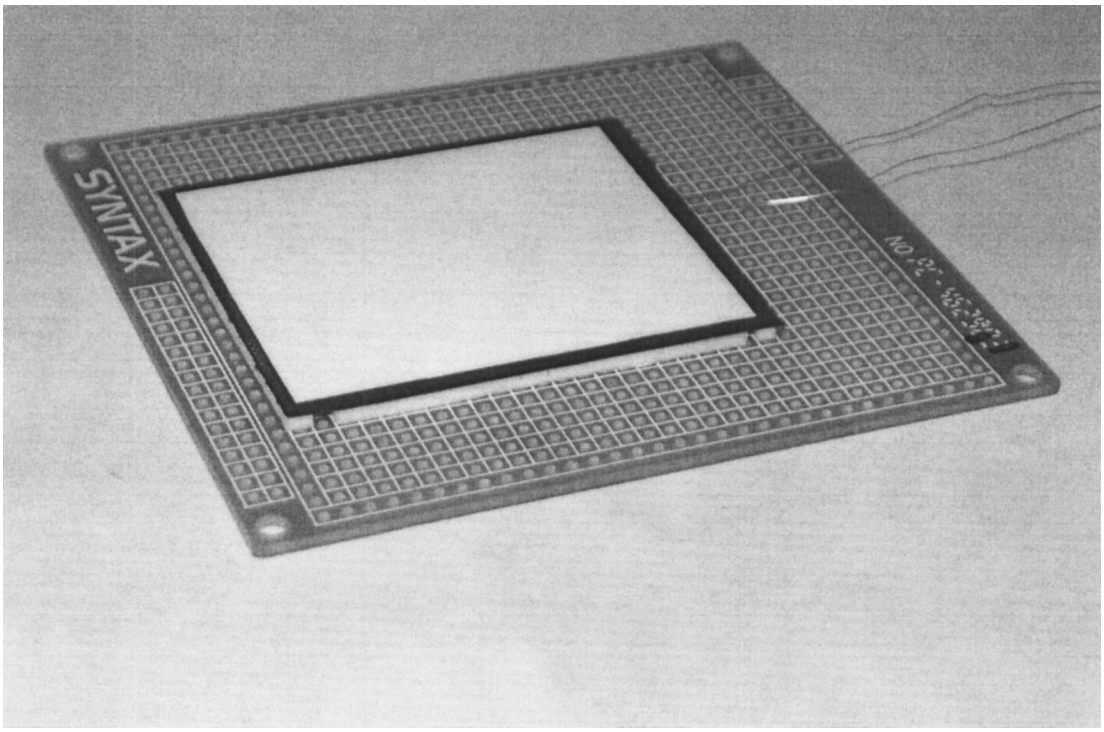

FIG. 8. Photo of the piezoelectric radiator No. 2.

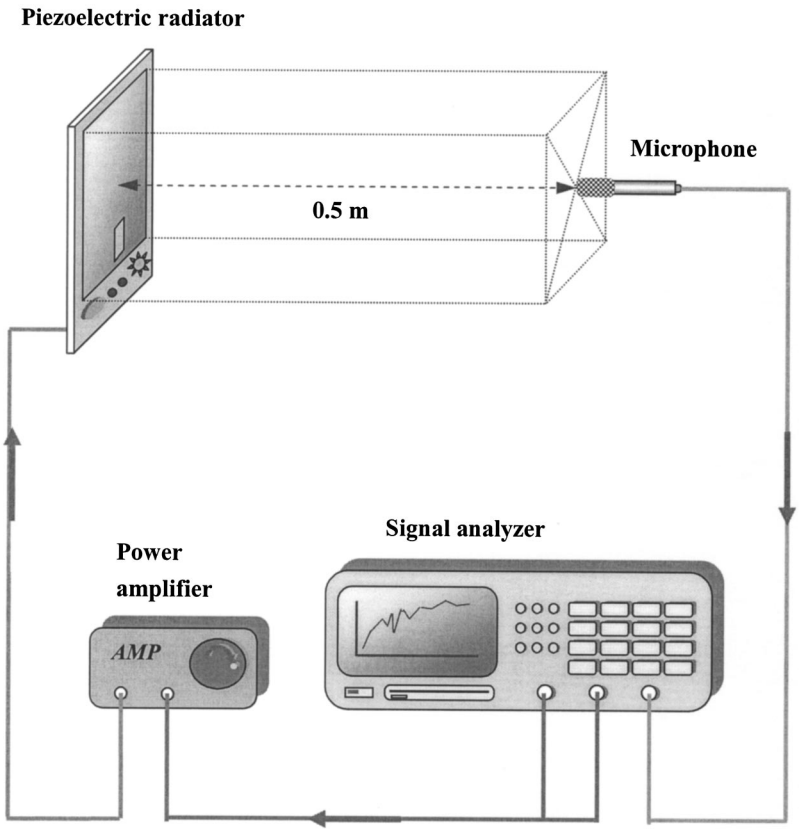

FIG. 9. The experimental arrangement for the performance measurement of the piezoelectric panel radiators. The measurement was conducted in an anechoic room.

A. Frequency responses of farfield pressure

The on-axis pressure responses at 0.5 m from panel speaker were measured. A random signal of 30 V rms, band-limited to 12.8 kHz was used as the input. Figures 10–12 illustrate the performance of various designs. Figure 10 shows the effect of the PZT positions. The design using the optimal position (No. 2) of the PZT produced a better low-frequency response than that using a nonoptimal position (No. 1). In Fig. 11, the frequency responses of the panel radiators, No. 2 and No. 3, are compared. The Young's modulus of the carbon fiber is close to the optimal value obtained from GA. The sound pressure level of the carbon fiber panel is higher than that produced by PC above 700 Hz, which results in a ''brighter'' sound quality of the carbon fiber radiator than the PC. In Fig. 12, we see the frequency responses of panel radiator No. 3 and No. 4. From the result,

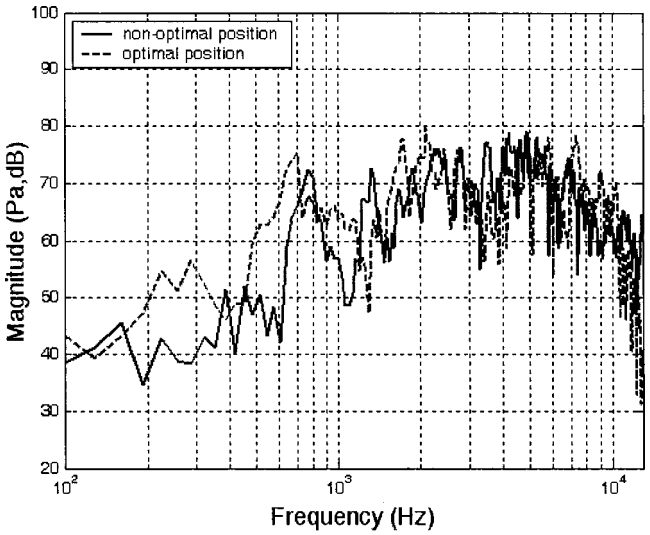

FIG. 10. The frequency responses of the panel radiators Nos. 1 and 2. The effect of the PZT positions on the panel is investigated. The design using the optimal position of the PZT produced a better low-frequency response than that using a nonoptimal position.

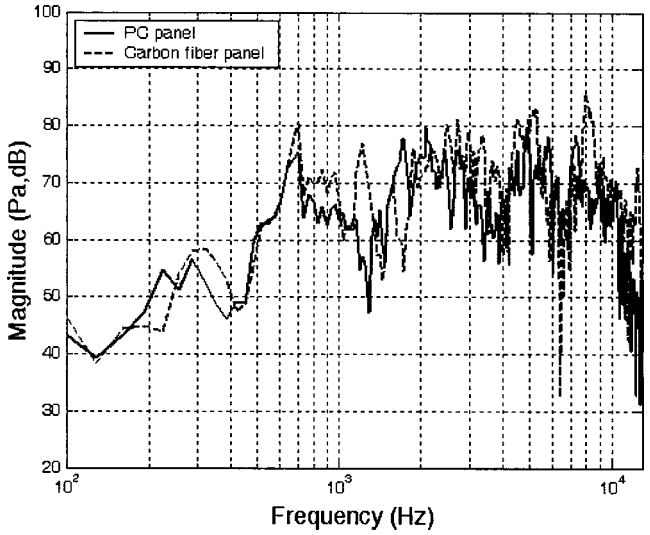

FIG. 11. The frequency responses of the panel radiators, Nos. 2 and 3. The effect of Young's modulus is investigated. The Young's modulus of the carbon fiber is close to the optimal value obtained from GA. The sound pressure level of the carbon fiber panel is higher than that produced by PC above 700 Hz.

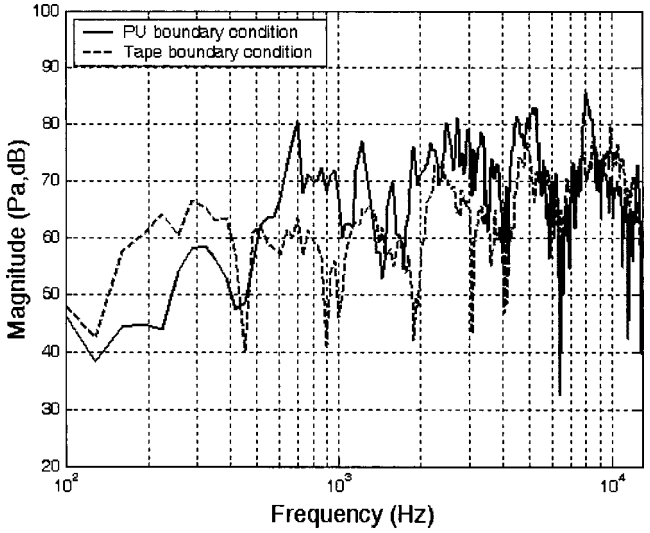

FIG. 12. The frequency responses of the panel radiator Nos. 3 and 4. The effect of the boundary condition is investigated. With a softer suspension, the low-frequency response is enhanced at the expense of the high-frequency output.

the profound effect of the boundary condition is also evidenced. With the soft suspension, the low-frequency response is enhanced at the expense of the high-frequency output.

B. Sensitivity

Sound pressure level is measured on-axis at the distance 0.5 m from the radiator, under the free-field condition. The input signal is the random noise of 30 V rms, bandlimited to 12.8 kHz, which amounts to the input electric power 0.018 W. The measured sensitivities of the No. 3 panel radiator is 76 dB. With this level of acoustic output, speech and music are found to be quite intelligible, even at 1 m distance.

C. Efficiency

The efficiency is defined as the ratio of the radiated acoustical power to the input electrical power. The input electrical power is calculated as

$$W_{\text{in}} \approx \frac{1}{2}\sum_{i=1}^{N} |V|^2 \frac{\text{Re}(Z)}{|Z|^2}\Delta f = \frac{1}{2}\sum_{i=1}^{N} P_{vv}\,\text{Re}\left(\frac{1}{Z}\right)\Delta f, \quad (69)$$

where V and Z are the Fourier transforms of the input voltage and the electrical impedance. P_{vv} is the power spectral density of the input voltage.

In this work, ISO 3745 was employed for measuring the radiated sound power in the anechoic room.[10] The measured efficiency of the No. 3 radiator was 0.767%. In order to appreciate this performance, a panel radiator using identical configurations, except a voice-coil exciter is used, was tested for comparison. The measured efficiency of the radiator driven by the voice-coil exciter was 0.075%. This impressive result indicates that the piezoelectric panel radiator is a very efficient device, which is indeed an attractive feature for many a power-saving applications.

D. Directional response

The directional response[11] of the panel radiator was measured by mounting the radiator on an automated turntable driven by a stepper motor. A 1/2 in. condenser microphone is placed at the distance 0.5 m from the radiator to measure the generated sound pressure under a free-field condition. The panel radiator was rotated at angles from 0° to 180°, with 1° increments. Random noise of 30 V rms, bandlimited to 12.8 kHz, served as the input. The measured results of directional response are shown in Fig. 13. The results indicate that the panel radiator has a relatively omnidirectional response. However, the directional responses are not symmetrical because the PZT is not mounted at the center position.

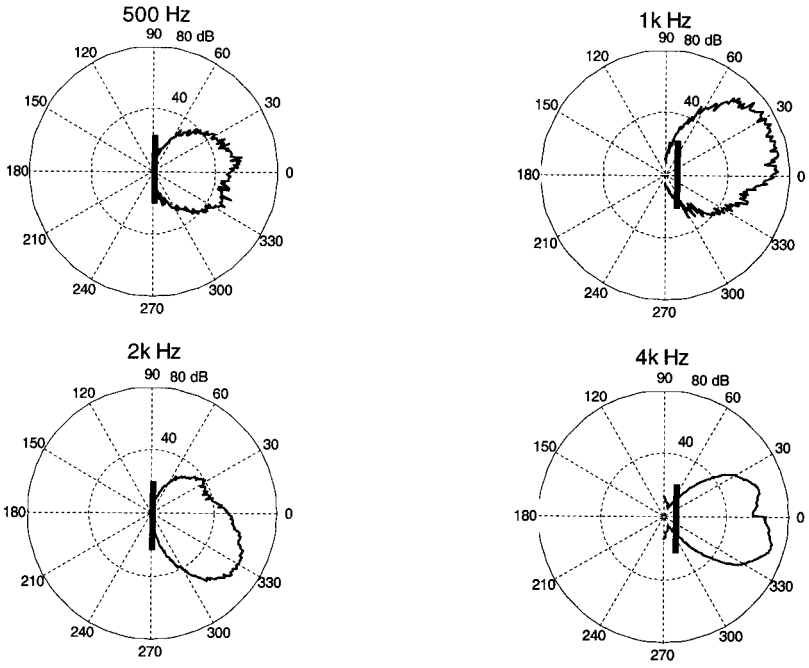

FIG. 13. Directional responses of the piezoelectric radiators at 500, 1, 2 and 4 kHz. The thick line at the center symbolizes the position of the panel.

VI. CONCLUSIONS

A piezoelectric radiator has been proposed in this paper. Although piezoelectrically driven radiators have been around for some time, these devices mainly exist in the form of narrow band acoustic radiators such as buzzers, sounders, sirens, etc., where sound quality is generally not of major concern. By contrast, this work developed an acoustic radiator for a different aim: to meet quality loudspeaker requirements with regard to speech and music listening. The reason why we used piezoelectricity as the driving mechanism lies in our emphasis on the 3C applications, where space and power consumption is critical.

Dynamic modeling of the system was carried out using the energy method and the assumed-modes method. A more elaborate approach than other study is exploited in modeling the acoustic loading and the model is established as a fully coupled system, which is important for a light structure considered here in the paper. Discretization is simplified by assuming a series expansion in energy terms, but not in partial differential equations. The assumed-modes method is employed in the series expansion such that the ensuing optimization process can be carried out in an efficient and practical way.

In this paper we seek to attain an optimal design of the piezoelectric panel speaker, using a ''synergetic'' approach. In particular, a nonconventional optimization algorithm, GA, was employed in this paper to effectively tackle this nonconvex problem. The GA is a multiple starting point algorithm and is not susceptible to the problem of local minima. Performance and adequacy as a broadband loudspeaker of the proposed device is thoroughly investigated. As confirmed by the numerical and experimental results of various indices, the piezoelectric radiator using the optimal configuration indeed produced better performance than the nonoptimal ones. The suspension, the material of the panel, and the mounting positions of PZT are important factors that may contribute to the performance of the radiators. The optimal combination of these parameters can be jointly considered in the GA procedure.

From the experimental investigation, the piezoelectric radiators produced quite impressive efficiency (approximately 10:1) over the panel speakers driven by voice-coil exciters. Furthermore, the thickness of present design of the piezoelectric radiator is 0.35 mm, which is significantly less than the 2.4 mm of the voice-coil panel speaker. In comparison with other conventional means, the piezoelectric radiators are found promising in meeting the increasingly stringent requirements of 3C products.

ACKNOWLEDGMENTS

Thanks are due to the illuminating discussions with NXT, New Transducers Ltd., UK. The work was supported by the *National Science Council (NSC)* in Taiwan, under Project No. NSC 89-2212-E009-057. Special thanks also go to Dr. Meng-Shiun Tsai in Chong-Cheng University for his helpful suggestions on derivations of piezoelectric plates.

[1] M. R. Bai and T. Huang, ''Development of panel loudspeaker system: Design, evaluation and enhancement,'' J. Acoust. Soc. Am. **109**, 2751–2761 (2001).
[2] H. Azima, ''NXT up against wall,'' Audio Magazine 34–41 (Sept., 1998).
[3] J. G. Smits, S. I. Dalke, and T. K. Cooney, ''The constituent equations of piezoelectric bimorphs,'' Sens. Actuators **28**, 41–61 (1991).
[4] J. W. Waanders, *Piezoelectric ceramics—Properties and Applications* (Philips Components Eindhoven, The Netherlands, 1991).
[5] H. L. Langhaar, *Energy Methods in Applied Mechanics* (Wiley, New York, 1962).
[6] H. F. Tiersten, *Linear Piezoelectric Plate Vibration* (Plenum, New York, 1969).
[7] L. Meirovitch, *Elements of Vibration Analysis* (McGraw-Hill, New York, 1986).
[8] A. P. Berkhoff, ''Sensor scheme design for active structural acoustic control,'' J. Acoust. Soc. Am. **108**, 1037–1045 (2000).
[9] J. H. Holland, ''Outline for a logical theory of adaptive system,'' J. Assoc. Comput. Mach. **3**, 297–314 (1962).
[10] ISO 3745, ''Acoustics—Determination of sound power levels of noise sources—Precision methods for anechoic and semi-anechoic rooms,'' 1977.
[11] L. L. Beranek, *Acoustics* (McGraw-Hill, New York, 1986).